HHS Public Access

Author manuscript

Mol Imaging Biol. Author manuscript; available in PMC 2023 May 16.

Published in final edited form as:

Mol Imaging Biol. 2022 August ; 24(4): 511–518. doi:10.1007/s11307-022-01708-2.

EGFR-targeted immunoPET of UMUC3 orthotopic bladder tumors

Tran T. Hoang[1,2], **Komal Mandleywala**[1], **Tara Viray**[1], **Kel Vin Tan**[1,3], **Jason S. Lewis**[1,2,4,5,6], **Patricia M. R. Pereira**[1]

[1]Department of Radiology, Memorial Sloan Kettering Cancer Center, New York, NY 10065, USA

[2]Department of Pharmacology, Weill Cornell Medical College, New York, NY 10065, USA

[3]Department of Diagnostic Radiology, LKS Faculty of Medicine, The University of Hong Kong, Hong Kong, China

[4]Molecular Pharmacology Program, Memorial Sloan Kettering Cancer Center, New York, NY 10065, USA

[5]Department of Radiology, Weill Cornell Medical College, New York, NY 10065, USA

[6]Radiochemistry and Molecular Imaging Probes Core, Memorial Sloan Kettering Cancer Center, New York, NY 10065, USA

Abstract

Purpose—Immuno Positron Emission Tomography (immunoPET) combines the specificity of an antibody with the sensitivity of PET to image dysregulated pathways in cancer. This study examines the performance of immunoPET using the radioimmunoconjugate [^{89}Zr]Zr-DFO-Panitumumab to detect epidermal growth factor receptor (EGFR) expression in an orthotopic model of bladder cancer (BCa).

Procedures—Expression and quantification of EGFR receptors were confirmed in four different BCa cell lines. Binding assays validated [^{89}Zr]Zr-DFO-Panitumumab specificity for EGFR-expressing UMUC3 BCa cells. Subcutaneous and orthotopic UMUC3 xenografts were then used for PET imaging and *ex vivo* biodistribution of the radioimmunoconjugate. Control cohorts included non-tumor mice, ^{89}Zr-labeled nonspecific IgG, and blocking experiments.

Results—[^{89}Zr]Zr-DFO-Panitumumab binds specifically to EGFR-expressing UMUC3 cells with a B_{max} value of 5.9×10^4 EGFRs/cell *in vitro*. ImmunoPET/CT images show localization of the antibody in subcutaneous UMUC3 xenografts and murine bladder tumors. In the

Corresponding authors: P.M.R Pereira; Current address: Department of Radiology, Washington University in St. Louis School of Medicine, St. Louis, MO 63110, USA; ribeiropereirap@wustl.edu; P: +1 314-273-4898; J. S. Lewis; lewisj2@mskcc.org P: +1 646-888-3038, Fax: 646-888-3059.

AUTHOR CONTRIBUTIONS

P.M.R.P. and J.S.L. designed the research; T.H., K.M., K.V.T., P.M.R.P., and J.S.L. wrote and reviewed the article; T.H., T.V., K.V.T., K.M., P.M.R.P., and J.S.L. acquired and analyzed data. All authors agreed to the manuscript to be published.

CONFLICT OF INTEREST STATEMENT

J. S. Lewis is an Editor-in-Chief for the Molecular Imaging and Biology journal. He recused himself from all aspects of the review of this manuscript and all decisions made in regard to revisions/acceptance.

orthotopic model, the immunoPET signal correlates with the respective tumor volume. *Ex vivo* biodistribution analysis further confirmed imaging results.

Conclusion—The preclinical data presents a proof of concept for utilizing EGFR-targeted immunoPET to image BCa with altered EGFR protein levels.

INTRODUCTION

Bladder cancer (BCa) is the fourth most common cancer type among men in the United States. BCa is increasingly associated with morbidity and mortality (1). The prevalence of BCa increases with age, with an average age of diagnosis between 70 and 84 years (2). Though this malignancy occurs mainly in older populations, the burden of bladder cancer can be reduced through early diagnosis and intervention, as disease progression is rapid and aggressive (3). Molecular imaging modalities are effective techniques in BCa diagnosis. In this context, computed tomography (CT), ultrasonography (US), and magnetic resonance imaging (MRI) have improved diagnostic accuracy in patients (4). However, phenotypic modifications that occur due to genomic aberrations and protein dysregulation during tumor development cannot be detected by CT, US, or MRI. Thus, immuno-positron emission tomography (immunoPET) is a promising imaging technique that provides phenotypic information regarding primary and metastatic lesions in BCa (5–7). Attractive characteristics of this technique include the sensitivity and quality derived from the PET technology and the targeting selectivity of the antibody for tumors based on the expression of the tumor-associated antigen (8, 9).

The antigen of interest in this study is the epidermal growth factor receptor (EGFR), a member of the HER family of receptor tyrosine kinases (RTKs) (10, 11). Under normal conditions, EGFR plays a critical role in tightly regulating the signaling pathways responsible for cell proliferation, differentiation, and survival. Under pathologic conditions, however, EGFR is frequently overexpressed and often mutated, contributing to cell proliferation, prevention of apoptosis, angiogenesis, cell motility, and metastasis in multiple cancer types, including BCa (12, 13). Previous studies have demonstrated that BCa cell lines have significant EGFR expression when compared with non-tumor urothelial cells (14). In patient samples, EGFR is overexpressed in up to 74% of BCa tissues (15) and low EGFR protein levels are reported for the normal urothelium (16). Notably, there is a positive correlation between EGFR expression levels and tumor progression and prognosis (17). As a result, EGFR has potential as a prognostic biomarker and therapeutic target for tumor diagnosis and inhibition, respectively.

In this study, the immunoPET probe consists of the anti-EGFR antibody Panitumumab labeled with the positron emitting isotope zirconium-89 (^{89}Zr). [^{89}Zr]Zr-DFO-Panitumumab was developed to detect EGFR expression in BCa. We have confirmed and quantified the binding specificity of the radioimmunoconjugate for the EGFR receptor *in vitro* and evaluated the capacity of the probe to image tumors in murine BCa models.

MATERIALS AND METHODS

Bladder cancer cell lines, cell culture, and Western blot

Human BCa cell lines UMUC3, RT112, T24, and UMUC4 were obtained from the American Type Culture Collection (ATCC Manassas, VA), Sigma-Aldrich, or the German Collection of Microorganisms and Cell Cultures. EGFR-overexpressing A431 epidermoid carcinoma cells were obtained from the ATCC. The cells were cultured according to the vendors' recommendations, authenticated at the Memorial Sloan-Kettering Cancer Center (MSKCC) integrated genomics operation core using short tandem repeat analysis, and used within a passage number of 8. The expression of EGFR in BCa cell lines or tumor extracts was determined by Western blot assays using the rabbit anti-EGFR antibody 1:1,000 (Abcam, #ab52894), as previously described (18).

Conjugation and radiolabeling of Panitumumab

Panitumumab was obtained from the MSK Hospital Pharmacy. To prepare [^{89}Zr]Zr-DFO-Panitumumab, the antibody was first conjugated with the bifunctional chelate *p*-isothiocyanatobenzyl-desferrioxamine (DFO-Bz-NCS; Macrocyclics, Inc), characterized by MALDI-TOF mass spectrometry (Supplementary Figs. 1,2 and Supplementary Table 1), and then labeled with zirconium-89 (^{89}Zr) (18–20). The [^{89}Zr]Zr-DFO-Panitumumab conjugates had a radiochemical purity of 99%, radiochemical yields ranging from 90–97% (Supplementary Fig. 3), molar activities in the range of 24.98–25.0 MBq/nmol, and immunoreactivities ranging from 92–95%. Molar activities were determined as previously reported (21). *In vitro* methods previously published by Lindmo *et al.* (22, 23) were used to determine the *in vitro* immunoreactivity in EGFR-overexpressing A431 cancer cells of the [^{89}Zr]Zr-DFO-Panitumumab conjugate prior to *in vivo* experimentation (Supplementary Fig. 4). [^{89}Zr]Zr-DFO-Panitumumab stability was above 90% after incubation in human serum at 37°C for a period of 100 h (Supplementary Fig. 5).

Binding, saturation-binding, and blocking assays

For the binding assays, UMUC3 cells were incubated with 37 KBq of ^{89}Zr-labeled Panitumumab (0.33–0.36 μg) for 1 h at 4 °C. Blocking experiments were performed by incubating cells with the radiolabeled antibody in the presence of 100-fold excess (33–36 μg) of unlabeled DFO-Panitumumab. The radioactivity from the supernatants and the cell pellet was then measured with a gamma counter, and immunoreactivity was calculated by dividing the radioactivity of the cell pellet by the sum of the radioactivity in the cell pellet and washing fractions.

For the saturation-binding assays, UMUC3 cells were incubated with [^{89}Zr]Zr-DFO-Panitumumab (0–128 nM) in PBS (pH 7.5) containing 1% (m/v) bovine serum albumin (Sigma) and 1% (m/v) sodium azide (Acros Organics) for 3 h at 4 °C. Unbound radioactivity was removed and cells were washed three times with PBS. The cells were solubilized in 100 mM NaOH, recovered, and the total cell-bound radioactivity was measured on a gamma counter calibrated for zirconium-89. Total binding was plotted versus the concentration of [^{89}Zr]Zr-DFO-Panitumumab; the data were fit via non-linear regression with a one-site binding model in GraphPad Prism 7.00 to determine B_{max}, K_D, and the non-specific binding

component. The ^{89}Zr-IgG non-specific component was subtracted from the total binding to generate specific binding curves.

UMUC3 subcutaneous and orthotopic xenografts

All experiments involving animals were performed according to the guidelines approved by the Research Animal Resource Center and Institutional Animal Care and Use Committee at MSKCC. UMUC3 cancer cells were inoculated subcutaneously or implanted into the bladder of 8–10 week-old *nu/nu* female mice (Charles River Laboratories), as previously described (24). Mice with orthotopic bladder tumors were monitored daily for any signs of pain or distress, and ultrasound imaging was used to monitor tumor development in murine bladders (Vevo 2100 Imaging System, Visualsonics) (24).

Small-animal positron emission tomography (PET) imaging and acute biodistribution studies

Mice bearing subcutaneous UMUC3 tumors (100–150 mm^3 in tumor volume) or orthotopic tumors were randomized before administering [^{89}Zr]Zr-DFO-Panitumumab or [^{89}Zr]Zr-DFO-IgG (8.25–9.18 MBq, 58–65 μg protein) by tail vein injection. PET imaging (n = 4 mice per group) and *ex vivo* biodistribution (n = 4 mice per group) were performed according to previously reported methods (18). PET images were analyzed using ASIPro VM software (Concorde Microsystems). Radioactivity present in each organ was expressed as the percentage of injected dose per gram of organ (% ID/g).

Statistical analysis

Data are expressed as mean ± S.E.M. Differences were analyzed by the Student t-test. The non-parametric one-tailed Spearman test was used to determine the correlation coefficient.

RESULTS

[^{89}Zr]Zr-DFO-Panitumumab binds EGFR-expressing BCa cells

Western blot analyzes were performed to determine EGFR expression in RT112, T24, UMUC3, and UMUC14 BCa cell lines (Fig. 1A). EGFR protein levels were comparable across the different BCa cell lines. When implanted in murine bladders, UMUC3 cells develop orthotopic tumors (24) that resemble the clinical condition of BCa (25), and were, therefore, the model of choice for subsequent imaging studies. To synthesize the immunoPET probe, Panitumumab was conjugated with DFO and then radiolabeled with zirconium-89. [^{89}Zr]Zr-DFO-Panitumumab was synthesized with radiochemical purity, radiochemical yields, and specific activities comparable to previous reports (18, 20, 26), 99%, 90–97%, and 24.98–25.0 MBq/nmol, respectively. *In vitro* studies demonstrated a positive correlation between UMUC3 BCa cell number and ^{89}Zr-labeled Panitumumab binding to cells (Fig. 1B). ^{89}Zr-labeled Panitumumab binding to 4 × 10^6 UMUC3 BCa cells was lower (Fig. 1B) compared with previously reported studies using similar cell numbers of EGFR-overexpressing A431 epidermoid carcinoma cells (20). Specificity of ^{89}Zr-labeled Panitumumab for UMUC3 cells was demonstrated using an excess of unlabeled Panitumumab (Fig. 1C). Next, the *in vitro* binding profile of ^{89}Zr-labeled Panitumumab was measured in a competitive radioligand saturation-binding assay (Supplementary Fig. 6, Fig.

1D). These results demonstrate that UMUC3 cells express 5.9×10^4 EGFRs/cell, which is lower than the number of EGFRs expressed per each A431 cell (2.0×10^6 EGFRs/cell as reported in ref. (27)). Altogether, these data indicate that [^{89}Zr]Zr-DFO-Panitumumab binds EGFR-expressing UMUC3 BCa cells.

[^{89}Zr]Zr-DFO-Panitumumab localizes in subcutaneous UMUC3 bladder xenografts

Based on our *in vitro* findings (Fig. 1), we next used PET imaging to monitor antibody-tumor binding and biodistribution of [^{89}Zr]Zr-DFO-Panitumumab in mice bearing subcutaneous UMUC3 xenografts. At 72 h after tail vein injection of ^{89}Zr-labeled Panitumumab, PET imaging demonstrated antibody accumulation in UMUC3 xenografts with minimal antibody accumulation in non-tumor murine bladders (Fig. 2A). Biodistribution of these mice at 72 h post administration of ^{89}Zr-labeled Panitumumab demonstrates average tumor percent-injected dose per gram (%ID/g) values of 15.05 ± 2.40 (Fig. 2B). Biodistribution studies demonstrate a favorable signal in the xenograft tissue relative to the non-tumor bladder with %ID/g values in murine bladders of 0.98 ± 0.20. The tumor uptake of a radiolabeled isotype control IgG is ~2-fold lower than Panitumumab (Supplementary Fig. 7). Additional biodistribution studies demonstrate higher %ID/g in [^{89}Zr]Zr-DFO-Panitumumab groups versus the block cohort (mice administered [^{89}Zr]Zr-DFO-Panitumumab in the presence of 2.3 mg of unlabeled Panitumumab, Fig. 2C).

[^{89}Zr]Zr-DFO-Panitumumab accumulates in murine tumor-bladders

^{89}Zr-labeled Panitumumab binds to UMUC3 cells (Fig. 1) and accumulates in UMUC3 subcutaneous tumors (Fig. 2). Therefore, immunoPET was used to image EGFR-expressing UMUC3 cells implanted in murine bladders (Fig. 3A). At 11 days after the cells' implantation in the bladder, ultrasound imaging could detect the presence of murine bladder tumors (Fig. 3A) and mice were intravenously administered ^{89}Zr-labeled Panitumumab. Mice without tumors were used as a negative control, receiving an intravenous injection of the immunoPET probe. Antibody-tumor uptake in bladder tumor cohorts was 2-fold higher when compared with no-tumor cohorts (Fig. 3B and Fig. 4A, C). When comparing %ID/g of the four different mice included in the tumor groups, Panitumumab accumulation in the tumors was highly variable from mouse to mouse (M1 = 5.10, M2 = 3.1, M3 = 3.8, M4 = 3.5 %ID/g; Fig. 3B, Fig. 4A). These observations are consistent with the varying growth rates and EGFR levels of UMUC3 BCa cells in murine bladders (Fig. 4B, D). Notably, Panitumumab accumulation in UMUC3 bladder tumors correlates with tumor volumes (Supplementary Fig. 8), bearing a Spearman's rank correlation coefficient (r) of 0.99 ($P = 0.0068$, Spearman's correlation). The uptake of a radiolabeled isotype control IgG in murine bladder tumors was 2-fold lower when compared with ^{89}Zr-labeled Panitumumab (Supplementary Table 2). Additional analyses in protein extracts of the orthotopic tumors of mice imaged with radiolabeled Panitumumab demonstrated similar EGFR protein levels in M1 and M3, although these mice showed a slightly different tumor volume. When compared with M3, M2 and M4 showed lower EGFR protein levels with similar tumor volumes and tumor-Panitumumab binding.

These results suggest that the antibody-tumor binding in these large tumors results from antibody binding to EGFR and other non-specific mechanisms such as enhanced permeability and retention (EPR) effects.

DISCUSSION

The ability of PET to visualize tumors based on tumor-specific markers has boosted the development of radiopharmaceuticals that use monoclonal antibodies or small molecules as carriers for the imaging tracer (28). FDG-PET is the most common PET tracer and allows visualization of primary tumors and metastases. However, FDG is not an ideal probe to image BCa, since FDG accumulation in the bladder can result from the small molecule renal excretion as well as tumor-specific accumulation. Intravesical administration of FDG shows low ability to delineate UMUC3 orthotopic bladder tumors (24). Our group has demonstrated the potential of PET in BCa using an antibody targeting carbohydrate-antigen (CA19.9) (5) and small molecules of carbohydrates (24). In the present study, we determined the potential of EGFR-targeted immunoPET to image BCa using an *in vivo* model mimicking the pattern of urinary bladder microtumor regrowth.

Aberrant activations of EGFR-mediated oncogenic signaling pathways compromise an effective therapeutic target for precision medicine approaches (11). Therapeutic monoclonal antibodies and tyrosine kinase inhibitors (TKIs) are EGFR-targeted therapies used in *KRAS* wild-type colorectal cancers (29) and EGFR-mutant tumors (30, 31). Targeting of EGFR signaling also has shown potential in bladder cancers (32–35). High levels of EGFR are reported in BCa, ranging from 27 to 74% (15). Different molecular and histopathological subtypes and heterogeneous cohorts account for variable EGFR expression in BCa (36). Therefore, immunohistochemical staining does not always predict therapeutic response to EGFR-targeted therapies (37). In this context, immunoPET is a powerful companion diagnostic for heterogeneous tumors.

Although EGFR overexpression occurs in BCa, EGFR-activating mutations are very low (15). Importantly, TKIs targeting EGFR in patients with BCa failed to show superior efficacy of combined chemotherapy when compared with chemotherapy alone (38). Because targeting EGFR expression with therapeutic monoclonal antibodies does not always correlate with efficacy, cytotoxic agents other than TKI are necessary for treating BCa. Anti-EGFR antibodies allow selective eradication of bladder tumor cells when labeled with cytotoxic radionuclides (33, 34, 39). Indeed, anti-EGFR antibodies radiolabeled with the alpha-particle emitter bismuth-213 (^{213}Bi) greatly decrease BCa growth in preclinical and clinical studies (33, 34, 39). Future studies will explore the efficacy of Panitumumab radioimmunotherapy in BCa. Although the diagnostic potential of ^{89}Zr-labeled Panitumumab has not been fully demonstrated, it represents a powerful technique to scout biodistribution of radioimmunotherapeutics (40), monitor tumor response to HER-targeted therapy (41), stratify patients for tumor-targeted therapies, and understand the interplay between EGFR tumoral levels and disease progression. Indeed, further experiments are planned in these directions.

Because urothelial carcinoma — also known as transitional cell carcinoma (TCC) — accounts for the most frequent type of BCa (42), this work used TCC bladder cancer cells. UMUC3 TCC cells, when implanted into murine bladders, develop tumors covering the urinary bladder that resemble the human disease (24, 43). However, tumors are established at a lower success rate after intravesical instillation than with a subcutaneous model (44). This contributes to differences in tumor volumes at the time of imaging studies related to the orthotopic model used in this study. Additionally, intravesical installation of human bladder cancer cells is limited to female mice due to challenging access of the male mouse urethra for catheterization. This represents a problem as the model does not mimic the human disease since BCa incidence is higher in men than in women. The substantial variability in orthotopic tumor growth between animals positively correlated with tumor uptake. For mice with large tumors, nonspecific antibody accumulation could also contribute for the differences in %ID/g observed in M1 versus M3, despite their similar levels in EGFR. Therefore, while ^{89}Zr-labeled Panitumumab can be used to visualize EGFR receptors in UMUC3 cells, its applicability *in vivo* is variable and depends on surface antigen density and EPR effects. The ability of this immunoPET approach to detect bladder tumors of small volume, as observed in M2 and M4, further supports the sensitivity of EGFR-targeted immunoPET.

Limitations of our study include the use of UMUC3 xenografts as the biological model. The 5.9×10^4 EGFR receptors per UMUC3 cell (Fig. 1D) makes for less density than that of models overexpressing EGFR (20) or when comparing with EGFR-overexpressing patient samples (14). The tumoral uptake of ^{89}Zr-labeled Panitumumab in A431 cancer cells, overexpressing 2 million EGFRs per cell (45), is 17.3 ± 0.3 %ID/g at 24 hours and rises to 32.90 ± 4.5 %ID/g at 120 hours (1). In our studies using mice with subcutaneous UMUC3 xenografts, ^{89}Zr-labeled Panitumumab yielded antibody-tumor uptakes of 15.05 ± 2.40 %ID/g at 72 h (Fig. 2B). Others have reported promising immunoPET results targeting receptors with a density comparable to the number of EGFRs in UMUC3 cells (46, 47). However, antibody-tumor accumulation in the orthotopic tumor model was lower when compared with the subcutaneous tumors (Fig. 4). It is possible that the use of an orthotopic BCa model containing a higher number of EGFR receptors could be a better biological model for our studies. Indeed, EGFR overexpression occurs more frequently in muscle-invasive BCa than with TCC (38), and further studies are planned in that direction. Other potential techniques to increase PET signal in the bladder tumor include the intravesical administration of the tracer (48). When used in a clinical setting, saturation of EGFR in normal tissues achieved by increasing the dose of the radioimmunoconjugate enhances the tumor-to-background signal (49).

CONCLUSIONS

The anti-EGFR Panitumumab antibody was radiolabeled with zirconium-89, resulting in an immunoPET probe with an affinity for EGFR-expressing BCa cells. ^{89}Zr-labeled Panitumumab binds specifically to UMUC3 BCa cells and allows visualization of EGFR-expressing BCa growing in murine bladders. Future studies in EGFR-overexpressing models of controlled BCa growth are necessary to fully validate the potential of radiolabeled

panitumumab or antibody fragments to provide information prior to, during, and after tumor-targeted therapies.

Supplementary Material

Refer to Web version on PubMed Central for supplementary material.

ACKNOWLEDGMENTS

The authors acknowledge the Radiochemistry and Molecular Imaging Probe Core, supported by NIH grant P30 CA08748. This study was supported in part by the Geoffrey Beene Cancer Research Center of MSKCC, NIH NCI R35 CA232130, NIH R01 CA244233-01A1. We gratefully acknowledge Mr. William H. and Mrs. Alice Goodwin and the Commonwealth Foundation for Cancer Research and The Center for Experimental Therapeutics of MSKCC. P.M.R. Pereira acknowledges the Tow Foundation Postdoctoral Fellowship from the MSKCC Center for Molecular Imaging and Nanotechnology, and the Alan and Sandra Gerry Metastasis and Tumor Ecosystems Center of MSKCC.

REFERENCES

1. Siegel RL, Miller KD, Jemal A. Cancer statistics, 2019. CA Cancer J Clin 2019;69(1):7–34. [PubMed: 30620402]
2. Lenis AT, Lec PM, Chamie K, Mshs MD. Bladder Cancer: A Review. JAMA 2020;324(19):1980–91. [PubMed: 33201207]
3. Grasso M Bladder Cancer: A major public health issue. Eur Urol Suppl 2008;7(7):510–5.
4. Wong VCK, Ganeshan D, Jensen CT, Devine CE. Imaging and management of bladder cancer. Cancers 2021;13(6).
5. Escorcia FE, Steckler JM, Abdel-Atti D, Price EW, Carlin SD, Scholz WW, et al. Tumor-specific ^{89}Zr immuno-PET imaging in a human bladder cancer model. Mol Imaging Biol 2018;20(5):808–15. [PubMed: 29508263]
6. Hughes ODM, Perkins AC, Frier M, Wastie ML, Denton G, Price MR, et al. Imaging for staging bladder cancer: a clinical study of ^{111}indium-labelled anti-MUC1 mucin intravenous monoclonal antibody C595. Bju Int 2001;87(1):39–46. [PubMed: 11121991]
7. Paquette M, Vilera-Perez LG, Beaudoin S, Ekindi-Ndongo N, Boudreaut PL, Bonin MA, et al. Targeting IL-5Ralpha with antibody-conjugates reveals a strategy for imaging and therapy for invasive bladder cancer. Oncoimmunology 2017;6(10):e1331195. [PubMed: 29123949]
8. Wei W, Rosenkrans ZT, Liu J, Huang G, Luo QY, Cai W. ImmunoPET: concept, design, and applications. Chem Rev 2020;120(8):3787–851. [PubMed: 32202104]
9. Deri MA, Zeglis BM, Francesconi LC, Lewis JS. PET imaging with (8)(9)Zr: from radiochemistry to the clinic. Nucl Med Biol 2013;40(1):3–14. [PubMed: 22998840]
10. Lemmon MA, Schlessinger J. Cell signaling by receptor tyrosine kinases. Cell 2010;141(7):1117–34. [PubMed: 20602996]
11. Yarden Y, Sliwkowski MX. Untangling the ErbB signalling network. Nat Rev Mol Cell Biol 2001;2(2):127–37. [PubMed: 11252954]
12. Nicholson RI, Gee JMW, Harper ME. EGFR and cancer prognosis. Eur J Cancer 2001;37:S9–S15. [PubMed: 11597399]
13. Seidl C Targets for therapy of bladder cancer. Semin Nucl Med 2020;50(2):162–70. [PubMed: 32172801]
14. Railkar R, Krane LS, Li QQ, Sanford T, Siddiqui MR, Haines D, et al. Epidermal Growth Factor Receptor (EGFR)-targeted Photoimmunotherapy (PIT) for the treatment of EGFR-expressing bladder cancer. Mol Cancer Ther 2017;16(10):2201–14. [PubMed: 28619755]
15. Chaux A, Cohen JS, Schultz L, Albadine R, Jadallah S, Murphy KM, et al. High epidermal growth factor receptor immunohistochemical expression in urothelial carcinoma of the bladder is not associated with EGFR mutations in exons 19 and 21: a study using formalin-fixed, paraffin-embedded archival tissues. Hum Pathol 2012;43(10):1590–5. [PubMed: 22406363]

16. Rotterud R, Nesland JM, Berner A, Fossa SD. Expression of the epidermal growth factor receptor family in normal and malignant urothelium. Bju Int 2005;95(9):1344–50. [PubMed: 15892828]
17. Mellon K, Wright C, Kelly P, Horne CHW, Neal DE. Long-term outcome related to epidermal growth-factor receptor status in bladder-cancer. J Urology 1995;153(3):919–25.
18. Pereira PMR, Mandleywala K, Ragupathi A, Lewis JS. Acute statin treatment improves antibody accumulation in EGFR- and PSMA-expressing tumors. Clin Cancer Res 2020;26(23):6215–29. [PubMed: 32998959]
19. Holland JP, Sheh Y, Lewis JS. Standardized methods for the production of high specific-activity zirconium-89. Nucl Med Biol 2009;36(7):729–39. [PubMed: 19720285]
20. Chang AJ, De Silva RA, Lapi SE. Development and characterization of ^{89}Zr-labeled panitumumab for immuno-positron emission tomographic imaging of the epidermal growth factor receptor. Mol Imaging 2013;12(1):17–27. [PubMed: 23348788]
21. Zeglis BM, Lewis JS. The Bioconjugation and Radiosynthesis of 89Zr-DFO-labeled Antibodies. JoVE 2015(96):e52521.
22. Lindmo T, Boven E, Cuttitta F, Fedorko J, Bunn PA Jr. Determination of the immunoreactive fraction of radiolabeled monoclonal antibodies by linear extrapolation to binding at infinite antigen excess. J Immunol Methods 1984;72(1):77–89. [PubMed: 6086763]
23. Lindmo T, Bunn PA, Jr. Determination of the true immunoreactive fraction of monoclonal antibodies after radiolabeling. Methods Enzymol 1986;121:678–91. [PubMed: 3523136]
24. Pereira PMR, Roberts S, Figueira F, Tome JPC, Reiner T, Lewis JS. PET/CT imaging with an ^{18}F-labeled galactodendritic unit in a galectin-1 overexpressing orthotopic bladder cancer model. J Nucl Med 2020;61(9):1369–75. [PubMed: 32005776]
25. van der Horst G, van Asten JJ, Figdor A, van den Hoogen C, Cheung H, Bevers RFM, et al. Real-Time Cancer Cell Tracking by Bioluminescence in a Preclinical Model of Human Bladder Cancer Growth and Metastasis. Eur Urol 2011;60(2):337–43. [PubMed: 21616583]
26. Nayak TK, Garmestani K, Milenic DE, Brechbiel MW. PET and MRI of metastatic peritoneal and pulmonary colorectal cancer in mice with human epidermal growth factor receptor 1-targeted ^{89}Zr-labeled panitumumab. J Nucl Med 2012;53(1):113–20. [PubMed: 22213822]
27. Haigler H, Ash JF, Singer SJ, Cohen S. Visualization by fluorescence of the binding and internalization of epidermal growth factor in human carcinoma cells A-431. Proc Natl Acad Sci U S A 1978;75(7):3317–21. [PubMed: 356052]
28. Herrmann K, Schwaiger M, Lewis JS, Solomon SB, McNeil BJ, Baumann M, et al. Radiotheranostics: a roadmap for future development. Lancet Oncol 2020;21(3):146–56.
29. Lievre A, Bachet JB, Le Corre D, Boige V, Landi B, Emile JF, et al. KRAS mutation status is predictive of response to cetuximab therapy in colorectal cancer. Cancer Res 2006;66(8):3992–5. [PubMed: 16618717]
30. Chen LF, Cohen EEW, Grandis JR. New strategies in head and neck cancer: understanding resistance to epidermal growth factor receptor inhibitors. Clin Cancer Res 2010;16(9):2489–95. [PubMed: 20406834]
31. Lynch TJ, Bell DW, Sordella R, Gurubhagavatula S, Okimoto RA, Brannigan BW, et al. Activating mutations in the epidermal growth factor receptor underlying responsiveness of non-small-cell lung cancer to gefitinib. New Engl J Med 2004;350(21):2129–39. [PubMed: 15118073]
32. Rose M, Maurer A, Wirtz J, Bleilevens A, Waldmann T, Wenz M, et al. EGFR activity addiction facilitates anti-ERBB based combination treatment of squamous bladder cancer. Oncogene 2021;39(7):6856–70.
33. Autenrieth ME, Seidl C, Bruchertseifer F, Horn T, Kurtz F, Feuerecker B, et al. Treatment of carcinoma in situ of the urinary bladder with an alpha-emitter immunoconjugate targeting the epidermal growth factor receptor: a pilot study. Eur J Nucl Med Mol Imaging 2018;45(8):1364–71. [PubMed: 29644393]
34. Fazel J, Rotzer S, Seidl C, Feuerecker B, Autenrieth M, Weirich G, et al. Fractionated intravesical radioimmunotherapy with ^{213}Bi-anti-EGFR-MAb is effective without toxic side-effects in a nude mouse model of advanced human bladder carcinoma. Cancer Biol Ther 2015;16(10):1526–34. [PubMed: 26177233]

35. Dominguez-Escrig JL, Kelly JD, Neal DE, King SM, Davies BR. Evaluation of the therapeutic potential of the epidermal growth factor receptor tyrosine kinase inhibitor gefitinib in preclinical models of bladder cancer. Clin Cancer Res 2004;10(14):4874–84. [PubMed: 15269164]
36. Knowles MA, Hurst CD. Molecular biology of bladder cancer: new insights into pathogenesis and clinical diversity. Nat Rev Cancer 2015;15(1):25–41. [PubMed: 25533674]
37. Chung KY, Shia J, Kemeny NE, Shah M, Schwartz GK, Tse A, et al. Cetuximab shows activity in colorectal cancer patients with tumors that do not express the epidermal growth factor receptor by immunohistochemistry. Journal of Clinical Oncology 2005;23(9):1803–10. [PubMed: 15677699]
38. Mooso BA, Vinall RL, Mudryj M, Yap SA, White RWD, Ghosh PM. The role of EGFR family inhibitors in muscle invasive bladder cancer: a review of clinical data and molecular evidence. J Urology 2015;193(1):19–29.
39. Pfost B, Seidl C, Autenrieth M, Saur D, Bruchertseifer F, Morgenstern A, et al. Intravesical alpha-radioimmunotherapy with ^{213}Bi-anti-EGFR-mAb defeats human bladder carcinoma in xenografted nude mice. J Nucl Med 2009;50(10):1700–8. [PubMed: 19793735]
40. Perk LR, Visser GWM, Vosjan MJWD, Stigter-van Walsum M, Tijink BM, Leemans CR, et al. ^{89}Zr as a PET surrogate radioisotope for scouting biodistribution of the therapeutic radiometals Y-90 and Lu-117 in tumor-bearing nude mice after coupling to the internalizing antibody cetuximab. J Nucl Med 2005;46(11):1898–906. [PubMed: 16269605]
41. Pereira PMR, Abma L, Henry KE, Lewis JS. Imaging of human epidermal growth factor receptors for patient selection and response monitoring - From PET imaging and beyond. Cancer Lett 2018;419:139–51. [PubMed: 29414302]
42. Iwata T, Kimura S, Abufaraj M, Janisch F, Karakiewicz PI, Seebacher V, et al. The role of adjuvant radiotherapy after surgery for upper and lower urinary tract urothelial carcinoma: A systematic review. Urol Oncol-Semin Ori 2019;37(10):659–71.
43. Naito T, Higuchi T, Shimada Y, Kakinuma C. An improved mouse orthotopic bladder cancer model exhibiting progression and treatment response characteristics of human recurrent bladder cancer. Oncol Lett 2020;19(1):833–9. [PubMed: 31885717]
44. Soloway MS, Masters S. Urothelial susceptibility to tumor cell implantation: influence of cauterization. Cancer 1980;46(5):1158–63. [PubMed: 7214299]
45. Fernandezpol JA. Epidermal growth-factor receptor of A431 cells - characterization of a monoclonal anti-receptor antibody noncompetitive agonist of epidermal growth-factor action. J Biol Chem 1985;260(8):5003–11. [PubMed: 2985573]
46. Burvenich IJG, Parakh S, Gan HK, Lee FT, Guo N, Rigopoulos A, et al. Molecular imaging and quantitation of EphA2 expression in xenograft models with ^{89}Zr-DS-8895a. J Nucl Med 2016;57(6):974–80. [PubMed: 26940768]
47. Sharma SK, Pourat J, Abdel-Atti D, Carlin SD, Piersigilli A, Bankovich AJ, et al. Noninvasive interrogation of DLL3 expression in metastatic small cell lung cancer. Cancer Res 2017;77(14):3931–41. [PubMed: 28487384]
48. Pool M, de Boer HR, Hooge MNL, van Vugt M, de Vries EGE. Harnessing integrative omics to facilitate molecular imaging of the human epidermal growth factor receptor family for precision medicine. Theranostics 2017;7(7):2111–33. [PubMed: 28638489]
49. Hoeben BA, Molkenboer-Kuenen JD, Oyen WJ, Peeters WJ, Kaanders JH, Bussink J, et al. Radiolabeled cetuximab: dose optimization for epidermal growth factor receptor imaging in a head-and-neck squamous cell carcinoma model. Int J Cancer 2011;129(4):870–8. [PubMed: 20957635]

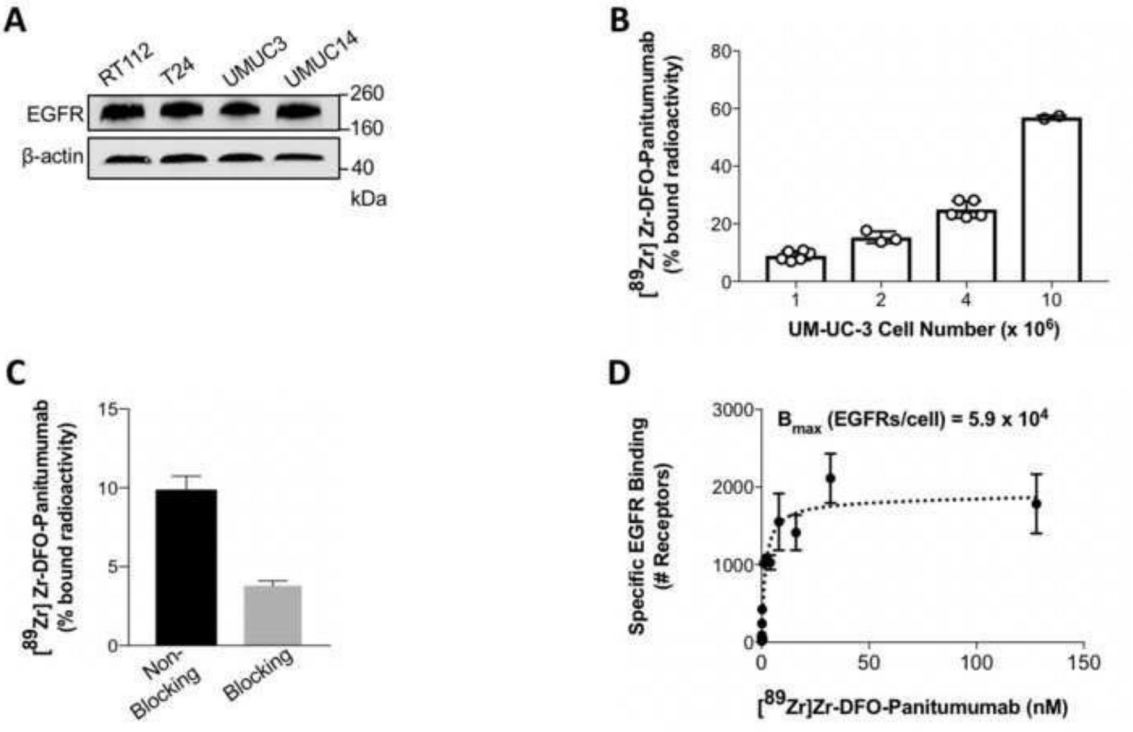

Figure 1.

(**A**) Western blot analysis of EGFR protein levels in RT112, T24, UMUC3, and UMUC14 bladder cancer cell lines. (**B, C**) ^{89}Zr-labeled Panitumumab binding to EGFR-expressing UMUC3 bladder cancer cells in the absence (**B**) and presence (**C**) of excess Panitumumab. UMUC3 bladder cancer cells (1, 2, 4, or 10 million) were incubated with 37 KBq of [^{89}Zr]Zr-DFO-Panitumumab (0.33–0.36 μg) for 1 h at 4°C. For blocking of ^{89}Zr-labeled Panitumumab binding to cancer cells, cells were incubated with ^{89}Zr-labeled Panitumumab in the presence of 33–36 μg DFO-Panitumumab. Data are presented as mean ± S.E.M, $n = 6$ (2 independent experiments). (**D**) UMUC3 cells were incubated with [^{89}Zr]Zr-DFO-Panitumumab (0–125 nM) for 3 h at 4°C. Specific binding of [^{89}Zr]Zr-DFO-Panitumumab and non-linear regression curve fit are represented in black spheres and dotted lines. Data are presented as mean ± S.E.M, $n = 3$.

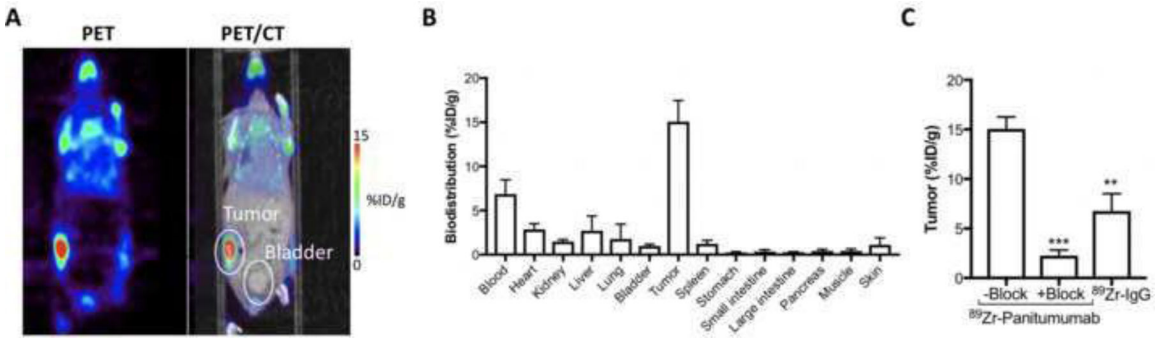

Figure 2.

(**A**) Representative coronal PET images and **(B)** biodistribution data of [^{89}Zr]Zr-DFO-Panitumumab in athymic nude mice bearing subcutaneous UMUC3 tumors. PET images and biodistribution were performed at 72 h after tail vein injection of [^{89}Zr]Zr-DFO-Panitumumab (8.25–9.18 MBq, 58–65 μg protein). Bars, $n = 4$ mice per group, mean ± S.E.M. (**C**) ^{89}Zr-labeled IgG or ^{89}Zr-labeled Panitumumab accumulation in UMUC3 subcutaneous tumors. Tumors were collected at 72 h after tail vein injection of [^{89}Zr]Zr-DFO-Panitumumab or [^{89}Zr]Zr-DFO-IgG (8.25–9.18 MBq, 58–65 μg protein). Blocking experiments were performed by administering [^{89}Zr]Zr-DFO-Panitumumab in the presence of 2.32 mg DFO-Panitumumab. Data are presented as mean ± S.E.M, $n = 4$ mice per group. $^{**}P < 0.01$, based on a Student's t-test. %ID/g, percentage of injected dose per gram.

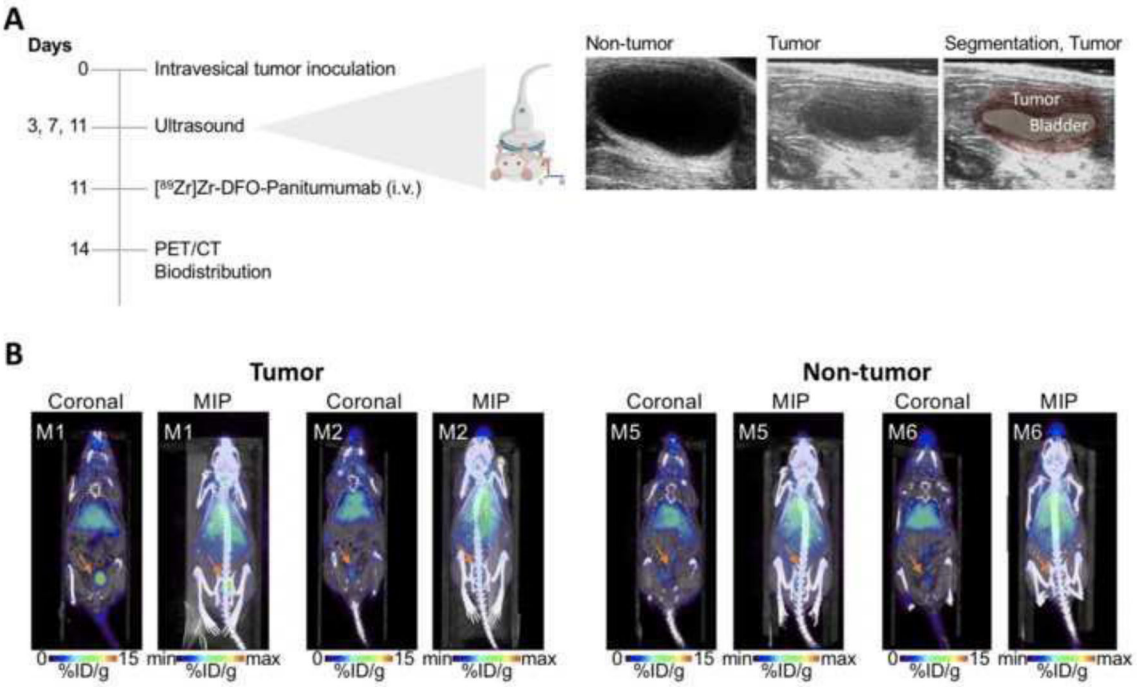

Figure 3.

(**A**) Schematic of PET imaging and biodistribution studies of [^{89}Zr]Zr-DFO-Panitumumab in orthotopic UMUC3 tumors. Right panel shows representative ultrasound images of murine bladders at 11 days after UMUC3 cells' implantation in the bladder. (**B**) Representative coronal and MIP PET images of [^{89}Zr]Zr-DFO-Panitumumab in athymic nude mice bearing orthotopic UMUC3 tumors or mice without tumors (M1, M2, M5, and M6 are mouse identifications of 2 mice included in the respective cohorts). PET images were collected at 72 h after tail vein injection of [^{89}Zr]Zr-DFO-Panitumumab (8.25–9.18 Mq, 58–65 μg protein). %ID/g, percentage of injected dose per gram.

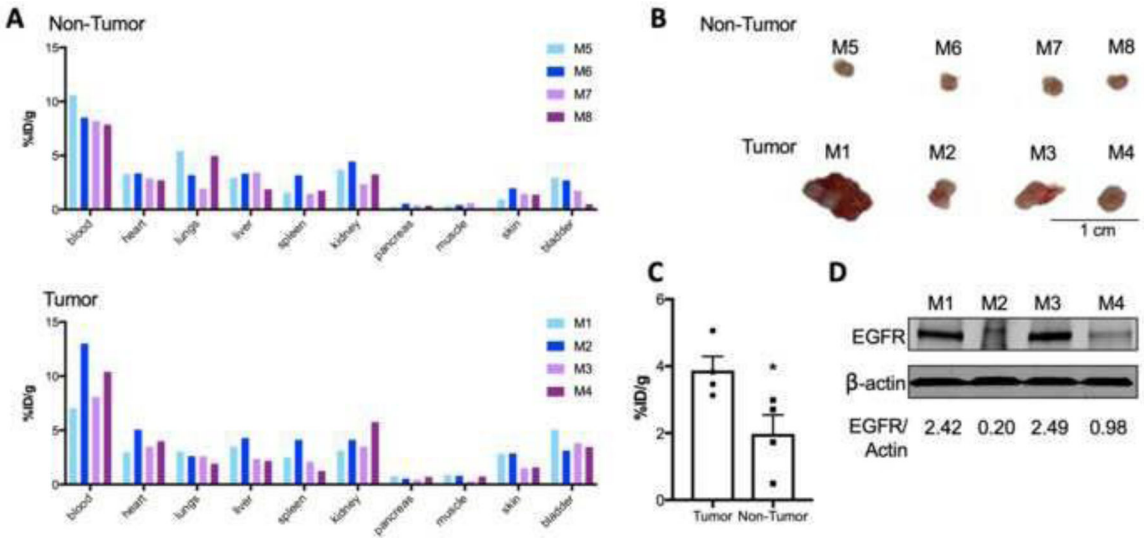

Figure 4.

(**A**) Biodistribution data of [^{89}Zr]Zr-DFO-Panitumumab in athymic nude mice without tumors (top panel, labeled as M5-M8 where each bar represents an individual mouse) or with UMUC3 orthotopic tumors (bottom panel, labeled as M1-M4 where each bar represents an individual mouse). Biodistribution was performed at 72 h after tail vein injection of [^{89}Zr]Zr-DFO-Panitumumab (8.25–9.18 MBq, 58–65 μg protein). Each bar represents data collected for one mouse of each cohort. (**B**) Bladder tumors at 14 days after UMUC3 cells' implantation in the bladder. (**C**) ^{89}Zr-labeled Panitumumab accumulation in UMUC3 orthotopic tumors or non-tumor bladders at 14 days after UMUC3 cells' implantation in the bladder. Bladders were collected at 72 h after tail vein injection of [^{89}Zr]Zr-DFO-Panitumumab (8.25–9.18 MBq, 58–65 μg protein). Data are presented as mean ± S.E.M, $n = 4$ mice per group. $^{*}P < 0.05$, based on a Student's t-test. (**D**) EGFR protein levels in UMUC3 orthotopic bladder tumors. Tumors were collected and EGFR expression analyzed by western blot for mice labeled as M1, M2, M3, and M4. β-actin is a loading control.